Cancer Imaging

RESEARCH

Open Access

Diffusion–based virtual MR elastography for predicting recurrence of solitary hepatocellular carcinoma after hepatectomy

Jiejun Chen[1,2,3†], Wei Sun[1†], Wentao Wang[1,2,3], Caixia Fu[4], Robert Grimm[5], Mengsu Zeng[1,2,3] and Shengxiang Rao[1,2,3*]

Abstract

Background To explore the capability of diffusion-based virtual MR elastography (vMRE) in the preoperative prediction of recurrence in hepatocellular carcinoma (HCC) and to investigate the underlying relevant histopathological characteristics.

Methods Between August 2015 and December 2016, patients underwent preoperative MRI examination with a dedicated DWI sequence (b-values: 200,1500 s/mm^2) were recruited. The ADC values and diffusion-based virtual shear modulus (μ_{diff}) of HCCs were calculated and MR morphological features were also analyzed. The Cox proportional hazards model was used to identify the risk factors associated with tumor recurrence. A preoperative radiologic model and postoperative model including pathological features were built to predict tumor recurrence after hepatectomy.

Results A total of 87 patients with solitary surgically confirmed HCCs were included in this study. Thirty-five patients (40.2%) were found to have tumor recurrence after hepatectomy. The preoperative model included higher μ_{diff} and corona enhancement, while the postoperative model included higher μ_{diff}, microvascular invasion, and histologic tumor grade. These factors were identified as significant prognostic factors for recurrence-free survival (RFS) (all $p < 0.05$). The HCC patients with μ_{diff} values > 2.325 kPa showed poorer 5-year RFS after hepatectomy than patients with μ_{diff} values ≤ 2.325 kPa ($p < 0.001$). Moreover, the higher μ_{diff} values was correlated with the expression of CK19 (3.95 ± 2.37 vs. 3.15 ± 1.77, $p = 0.017$) and high Ki-67 labeling index (4.22 ± 1.63 vs. 2.72 ± 2.12, $p = 0.001$).

Conclusions The μ_{diff} values related to the expression of CK19 and Ki-67 labeling index potentially predict RFS after hepatectomy in HCC patients.

†Jiejun Chen, Wei Sun and Wentao Wang contributed equally to this work.

*Correspondence:
Shengxiang Rao
raoxray@163.com
[1]Department of Radiology, Zhongshan Hospital, Fudan University, No. 180 Fenglin Road, Xuhui District, Shanghai 200032, China
[2]Shanghai Institute of Medical Imaging, Shanghai, China
[3]Department of Cancer Center, Zhongshan Hospital, Fudan University, Shanghai, China
[4]MR Application development, Siemens Shenzhen Magnetic Resonance Ltd, Shenzhen, China
[5]MR Application Predevelopment, Siemens Healthineers AG, Erlangen, Germany

Introduction

Hepatocellular carcinoma (HCC) is the most common primary malignant tumor of the liver which ranked as the third leading cause of cancer-related death worldwide [1]. Although great progress has been made in the early diagnosis and surgical techniques of HCC, the prognosis of HCC is still very poor, the tumor recurrence rate is up to 80% for patients who received curative resection [2]. Previous studies have reported that some specific factors are associated with the recurrence of HCC, including microvascular invasion (MVI), cytokeratin 19 (CK19) expression, high Ki-67 labeling index and poor histologic differentiation etc. [3–6]. However, these factors can only be identified by the post-operative histopathological examinations. Preoperative identification of patients at high risk for recurrence may improve individualized management and reach better prognosis.

In clinical practice, CT and MRI play an important role in the diagnosis, staging and prognostic evaluation of HCC [7]. However, non-invasive imaging techniques are known to experience difficulties in predicting recurrence of HCC. In addition to morphologic imaging features and dynamic enhancement patterns, tumor stiffness may be used as a prognostic factor, which is regarded as be correlated with the degree of tumor cellularity and fibrosis. Magnetic resonance elastography (MRE) is a useful tool for noninvasive evaluation of tumor stiffness for liver tumor characterization [8]. Previous studies have reported that the MRE-based stiffness could be used as a potential biomarker for predicting HCC recurrence after surgical resection [9]. However, the application of MRE was limited by the need for external mechanical setup and dedicated MRI sequence. Recently, a novel technique named diffusion-weighted imaging (DWI)-based virtual elastography (vMRE) was proposed by Le Bihan et al. [10]. Compared with traditional DWI, the vMRE is proposed on the basis of two b-values (200 and 1500 s/mm^2). By introducing these higher b-values to the mono-exponential model, the vMRE can reveal both Gaussian and non-Gaussian diffusion with theoretically optimized sensitivity. With the enhanced sensitivity to tissue microstructure, previous studies have reported that the so-called shifted apparent diffusion coefficient (sADC) parameter obtained from vMRE has equivalent diagnostic efficacy of liver fibrosis staging as conventional MRE [11]. Moreover, the vMRE can be applied without the need of additional hardware. Since the HCC lesions in patients with recurrence may present with increased cellularity and stiffness, the vMRE might have potential value in the tumor characterization of HCC. To the best of our knowledge, the vMRE has seldom been applied for liver tumors.

Therefore, the purpose of this study is to explore the capability of the parameters obtained from vMRE in the preoperative evaluation of tumor recurrence and underlying relevant histopathological characteristics in HCC patients.

Materials and methods

This study is a retrospective analysis of patients from a prospective cohort. Our institutional review board approved the analysis of the MRI data and written informed consent was obtained from all patients.

Patients

Between August 2015 and December 2016, a total of 128 consecutive patients suspected of hepatic lesions were included. The inclusion criteria were as follows: [1] preoperative DWI sequence including at least 2 b values (200 and 1500 s/mm^2) and contrast enhanced MR images were acquired; [2] the interval between MR examination and hepatectomy was within 7 days; [3] patients have no prior treatments with hepatic lesions. The exclusion criteria were as follows: (1) histopathological results disprove the diagnosis of HCC; (2) insufficient image quality caused by susceptibility artifacts or respiratory motion; (3) the diameter of lesions was less than 1 cm; (4) patients with more than one HCC lesion. Finally, 87 patients with solitary HCC lesions were enrolled in this study. The flowchart of patient's selection process is displayed in Fig. 1.

Imaging acquisition

All MR images were obtained by using a 1.5T MR system (MAGNETOM Aera; Siemens Healthineers, Erlangen, Germany). Diffusion-weighted MR imaging was performed with a single-shot spin-echo echo-planar (ss-EPI) sequence. The detailed parameters were as follows: repetition time (TR) /echo time: 8000 ms/63 ms, field of view, 380×308 mm^2; matrix, 128×128; section thickness, 5 mm; b-values: 0, 200, 500 and 1500 s/mm^2 with a number of averages of 1, 1, 2, 3; diffusion model: 3-scan trace. The total scan time for the DWI protocol was about 2 min and 30s. Other clinical routine MR sequences including a T2-weighted sequence with fat suppression, 3D T1-weighted (in-phase and out-of-phase) volumetric interpolated breath-hold examination (VIBE), and a dynamic 3D T1-weighted VIBE examination was performed before and after the injection of contrast media. The arterial phase, portal venous phase, and equilibrium phase images were obtained at 20–30 s, 70–80 s, and 180 s after injection of 0.1 mmol/kg gadopentate dimeglumine (Magnevist; Bayer Schering Pharma AG, Berlin, Germany) at a rate of 2 mL/sec, respectively. The detailed MR scan parameters are displayed in Table 1.

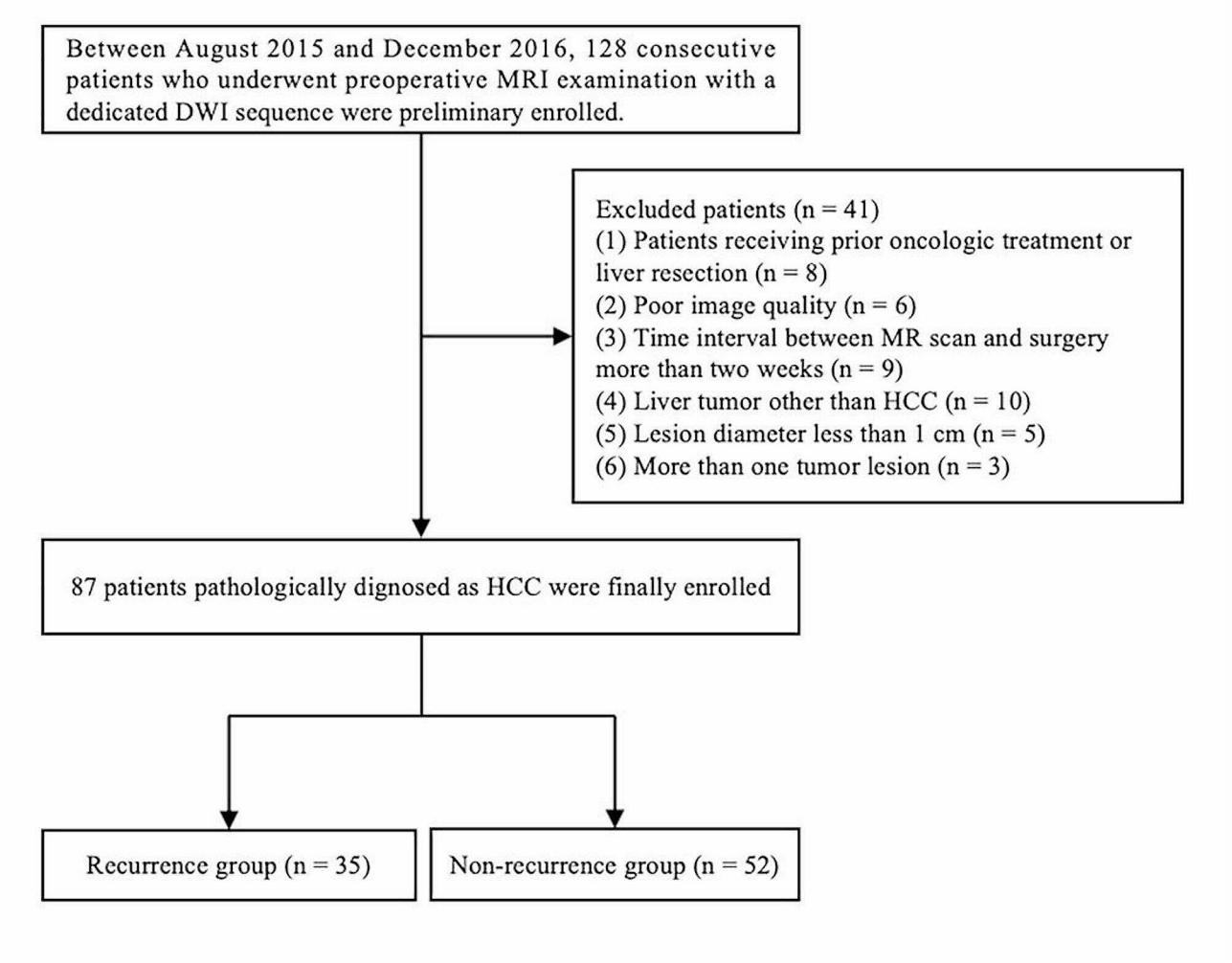

Fig. 1 Flow diagram shows inclusion and exclusion criteria in this study
MRI: magnetic resonance imaging; HCC: hepatocellular carcinoma

Table 1 The parameters of MRI scan protocol

Parameter	DWI	In/out of phase T1-weighted imaging	T2-weighted imaging	T1-weighted VIBE sequence
Repetition time (ms)	8000	6.87	2400	4.36
Echo time (ms)	63	2.38/4.76	94	2
Field of view (mm^2)	380×308	380×278	380×308	380×297
Scan matrix	128×128	320×240	320×224	320×240
Slice thickness (mm)	5	4	5.5	3
Gap (mm)	1	0	1.1	0

DWI: diffusion-weighted imaging; VIBE: volumetric interpolated breath-hold examination

Imaging analysis

Before ADC and sADC were calculated using an in-house developed program based on MATLAB (Mathworks, Natick, Mass), motion registration was performed for the original DWI images with 4 b-values by using a research application (MR Multiparametric Analysis; Siemens Healthineers). The ADC was calculated based on the following formula:

$$\mathrm{ADC}\ (\mathrm{mm}^2/\mathrm{s}) = \ln(S_0/S_{500})/500$$

Where S_{500} and S_0 are the signal intensity when b-values of 500 and 0 s/mm^2 are applied, respectively.

The shifted apparent diffusion coefficient (sADC) was calculated by using the following formula with two key b values (200 and 1500 s/mm^2) which was optimized to reflect Gaussian and non-Gaussian diffusion [10].

$$\mathrm{sADC}\ (\mathrm{mm}^2/\mathrm{s}) = \ln(S_{200}/S_{1500})/1300$$

Where S_{200} and S_{1500} are the signal intensity when b-values of 200 and 1500 s/mm^2 are applied, respectively. After sADC was calculated, the diffusion-based shear modulus (μ_{diff}) was then obtained based on the following formula proposed by previous research [10]:

$$\mu_{diff}\ (\mathrm{kPa}) = \alpha\ \mathrm{sADC} + \beta$$

where α and β are two constants with values of -12,740 and 14.0, respectively.

All images were analyzed by two independent observers who are blinded to histopathologic and follow-up results. The region of interest (ROI) was outlined in ITK-SNAP for the whole tumor on the DW images of b200, with contrast-enhanced MR images as reference. Furthermore, we also evaluate the background normal hepatic parenchyma by using a total of 3 round ROI of the same extent (100 mm^3) on the EPI-DWI images of b200, avoiding large vessels and bile ducts, lesions, or artifacts. Then the ROI was simultaneously copied to ADC, sADC and μ maps to generate mean values of ADC, sADC and μ for final analysis. Mean values of the quantitative parameters of the background liver parenchyma were calculated by averaging the measurements of the 3 ROIs. Thirty cases were randomly selected to test the reproducibility of the quantitative parameters.

MR morphologic features

Two independent radiologists who were blinded to the histopathological results reviewed all MR images in the picture archiving and communication system (PACS). In addition to tumor size, the following morphologic features based on the LI-RADS ver.2018 diagnostic algorithm were evaluated: (1) tumor diameter, (2) tumor margin (classified as smooth margin or non-smooth margin), (3) targetoid appearance on DWI or contrast-enhanced images (including rim arterial phase hyperenhancement, peripheral washout and delayed central enhancement), (4) corona enhancement (defined as the hyperperfusion of liver tissue surrounding the tumor border in late arterial phase or early portal venous phase), (5) intratumoral hemorrhage, and (6) intratumoral fat deposition. The representative images of the MR features are displayed in Supplementary Table S1. When there was a disagreement between the two observers, a consensus would be reached through discussion.

Histopathological examination and follow-up

Pathological characteristics of surgical resection specimens such as Edmondson-Steiner grade, presence of microvascular invasion (MVI) of tumor, satellite lesions et al. were evaluated and confirmed by a team of experienced pathologists (each with more than 10 years of experience). The expression status of CK19, CD34, CD7 and Gglypican-3 (GPC3) were determined as positive or negative by immunohistochemical staining. In particular, 5% was used as a cutoff value for identifying positive CK19 by using previous research as references [12]. Furthermore, low expression of Ki-67 was defined as ≤30% tumor cells were positive, while high expression of Ki-67 was defined as >30% tumor cells were positive. MVI was defined as tumor emboli in a vascular space lined by endothelium cells on microscopy [13]. The histological grade of HCC was determined according to the Edmondson-Steiner classification and Edmondson-Steiner grade I and II were classified into the low-grade group, grade III and IV were classified into the high-grade group. After surgical resection, patients were followed up with ultrasonography and/or contrasted computed tomography or MRI every 3 months in the first year and every 3–6 months after first year to assess tumor progression. The recurrence-free survival (RFS) was recorded, which was defined as the length of time from the date of hepatectomy to the date of any type of initial tumor recurrence until December 31, 2022.

Statistical analysis

Continuous variables were analyzed using the independent t-test or Mann-Whitney U test depending on normality test. Categorical variables were analyzed by the chi-square test or Fisher's exact test. Spearman correlation coefficients were calculated to assess the correlation between quantitative parameters and histologic fibrosis scores. The interobserver agreement was evaluated using intraclass correlation coefficient (ICC) for continuous parameters (≤0.2, poor; 0.2–0.4, fair; 0.4–0.6, moderate; 0.6–0.8, good; 0.8–1.0, excellent). The best cutoff value for vMRE-derived parameter was determined based on receiver operating characteristic (ROC) curves. Univariate and multivariate regression analysis was performed to identify independent predictors of recurrence using a Cox proportional hazards model. Univariate analysis was firstly performed and then those parameters showed statistical significance in univariate analysis were used for further stepwise multivariate Cox regression analysis. The Kaplan-Meier method was used to evaluate the recurrence rate and comparison between groups was accessed by using the log-rank test. Finally, the ROC curve and area under the ROC curve (AUC) were used to assess the diagnostic performance of significant variables for predicting recurrence after hepatectomy. The SPSS software (version 26.0) and R software (version 3.6.1) were used for all statistical analysis. A two-sided *P* value less than 0.05 was considered statistically significant.

Results

Patient characteristics and follow-up findings

Baseline demographic and clinical characteristics of patients are listed in Table 2. The final study included 87 patients (70 men and 17 women; mean age, 53.7 ± 9.7 years) with solitary HCC. Among all the study population, 35 patients (40.2%) were found to have recurrence after hepatectomy during the whole follow-up period (range 2–60 months; median, 27 months). The median time interval between hepatectomy and HCC recurrence was 18 months (range 2–59 months). The most predominant cause of the underlying liver disease was the chronic hepatitis B viral infection (96.6% of patients). Among pathological features, the HCC lesions in patients with recurrence were more likely to demonstrated MVI ($p<0.001$) and higher histological tumor grade ($p=0.012$) than those without. The remaining baseline characteristics of HCC patients with or without recurrence showed no statistical difference.

Quantitative MR characteristics measurements

Among all the quantitative parameters, the HCC lesions in patients with recurrence demonstrated significantly higher μ_{diff} values compared with those in patients without recurrence (4.27 ± 1.96 vs. 2.60 ± 1.89, $p<0.001$). However, the ADC values showed no statistical differences between these two groups (1.40, interquartile range (IQR):1.31–1.57 vs. 1.51, IQR:1.30, 1.60, $p=0.257$) (Figs. 2 and 3). In terms of background liver parenchyma, the μ_{diff} value of the background liver ($\mu_{diff-liver}$) increased with increasing liver fibrosis stage (rho = 0.563, $p<0.001$). However, the ADC value was not correlated with liver fibrosis stage (rho = -0.174, $p=0.107$). The AUC of $\mu_{diff-liver}$ value in diagnosing liver fibrosis stage 3 or greater is 0.778. In the thirty randomly selected cases,

Table 2 Clinical characteristics of 87 HCC patients

Variable	Total (n = 87)	Recurrence (*n* = 35)	Non-recurrence (n = 52)	*P* Value
Gender				0.929
Male	70 (80.5)	28 (80.0)	42 (80.8)	
Female	17 (19.5)	7 (20.0)	10 (19.2)	
Age (years)*	53.7 ± 9.7	54.2 ± 9.4	53.0 ± 10.2	0.565
Total bilirubin > 20.4 μmol/L	13 (14.9)	7 (20.0)	6 (11.5)	0.278
Direct bilirubin > 6.8 μmol/L	28 (32.2)	14 (40.0)	14 (26.9)	0.261
Alanine aminotransferase level > 50 U/L	18 (18.0)	7 (20.0)	11 (21.2)	0.896
Aspartate aminotransaminase level > 40 U/L	27 (31.0)	11 (31.4)	16 (30.8)	0.948
γ-glutamyltransferase > 60 U/L	45 (51.7)	18 (51.4)	27 (51.9)	0.964
AFP > 20 ng/ml	50 (57.4)	17 (48.5)	32 (61.5)	0.232
Carcinoembryonic antigen > 5 ng/ml††	11 (12.6)	3 (8.6)	8 (15.4)	0.543
Cancer antigen 19 – 9 > 34 U/ml	26 (29.9)	12 (34.3)	14 (26.9)	0.462
Aetiology of liver disease†				> 0.99
Hepatitis B Virus	84 (96.6)	34 (97.1)	50 (96.2)	
Hepatitis C Virus	1 (1.1)	1 (2.9)	0 (0)	
None or other	2 (2.3)	0 (0)	2 (3.8)	
BCLC stage				0.311
BCLC 0	11 (12.6)	6 (17.1)	4 (1.92)	
BCLC A	76 (87.4)	29 (82.9)	48 (92.3)	
Tumor size††	4.0 (2.6, 6.0)	4.5 (2.6, 7.3)	4.0 (2.6, 4.9)	0.247
MVI				< 0.001
present	13 (14.9)	12 (34.3)	1 (1.9)	
absent	74 (85.1)	23 (65.7)	51 (98.1)	
Edmondson-Steiner grade				0.012
G1-G2	52 (59.8)	14 (40.0)	35 (67.3)	
G3-G4	35 (40.2)	21 (60.0)	17 (36.7)	
Fibrosis stage				0.341
F0-F2	30 (34.5)	10 (28.6)	20 (38.5)	
F3-F4	57 (65.5)	25 (71.4)	32 (61.5)	

Unless otherwise specified, data are numbers of patients with percentages in parentheses

* Data are means ± standard deviation and compared by using the independent t-test

† Data are compared by using the Fisher exact test

†† Data are means with the interquartile range in parentheses and compared by using Mann–Whitney U test

AFP: alpha-fetoprotein; BCLC: barcelona clinic liver cancer; MVI: microvascular invasion

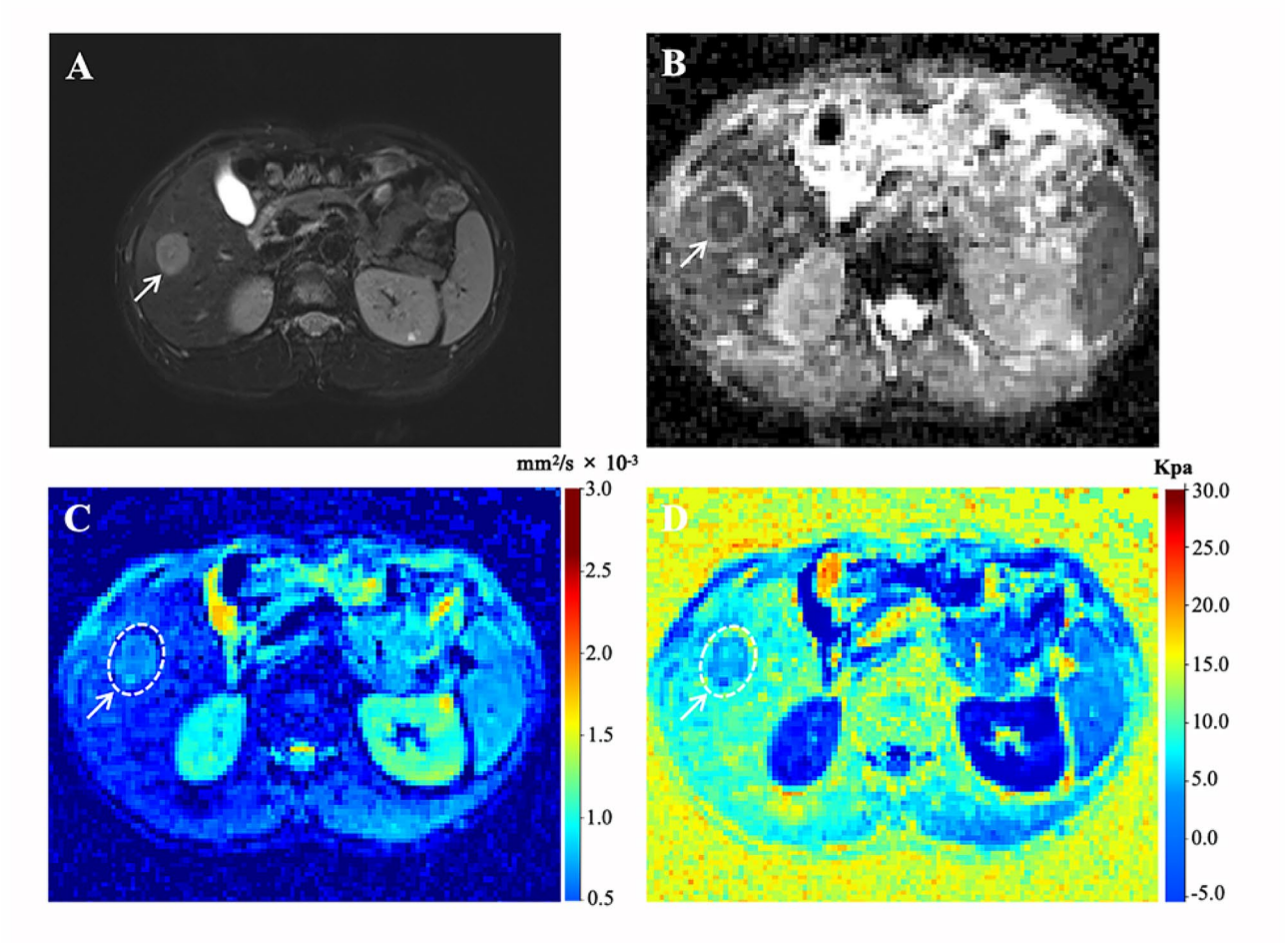

Fig. 2 Representative MR images of a 47-year-old man with pathologically verified HCC. Tumor recurrence occurred 13 months after surgery. (**A**) Axial T2-weighted image showing a hyperintensity mass (arrow) on segment VI of the liver. (**B**-**D**) ADC, sADC, and μ_{diff} maps showing that the mean ADC, sADC, and μ_{diff} values of the tumor (arrow) were 1.44×10^{-3} mm^2/s, 0.70×10^{-3} mm^2/s, and 5.10 kPa, respectively. ADC, apparent diffusion coefficient; sADC, shifted apparent diffusion coefficient; μ_{diff}, DWI-based virtual shear modulus

the agreements of quantitative parameters between two observers were excellent for ADC, μ_{diff}, ADC_{liver} and $\mu_{diff-liver}$, with ICC of 0.929 (95% confidence interval (CI): 0.860–0.965), 0.935 (0.870–0.969), 0.829 (0.687–0.911) and 0.867 (0.741–0.935), respectively.

Univariate and multivariate Cox analyses for predictors of RFS

In the univariate analysis, the μ_{diff}*values*, corona enhancement, target appearance, tumor grade, MVI and high KI-67 labeling index were significantly associated with RFS (all $p<0.05$). All the parameters were employed for building the postoperative model including clinic-pathologic and radiologic features. The pathological parameters including tumor grade, MVI and KI-67 labeling index can be obtained only after the operation, therefore they were excluded in the multivariable analysis for establishing the preoperative model. In the subsequent multivariable analysis of Cox proportional hazards regression, independent parameters were identified for both models (Table 3). Since the μ_{diff} values were identified as the independent risk factors of HCC recurrence in both preoperative and postoperative models, the patients were stratified into a high μ_{diff} values (>2.325 kPa) group and a low μ_{diff} values (≤2.325 kPa) group. The Kaplan–Meier method and log-rank test revealed that the 5-year RFS after hepatectomy were significantly shorter in the higher μ_{diff} values group compared to the lower μ_{diff} values group. The 1-year, 3-years, and 5-years cumulative recurrence rates of patients with high μ_{diff} values were 20.1%, 45.7%, 71.5%, respectively and 6.8%, 14.1%, 14.1%, respectively, in the group of patients with low μ_{diff} values (Fig. 4, $p<0.001$). The ROC curve of the risk factors selected by Cox regression analysis are displayed in Fig. 5. The AUC of μ_{diff} values, preoperative model and postoperative model were 0.731, 0.773 and 0.836, respectively. The postoperative model demonstrated the best diagnostic efficiency which is significantly higher than using μ_{diff}

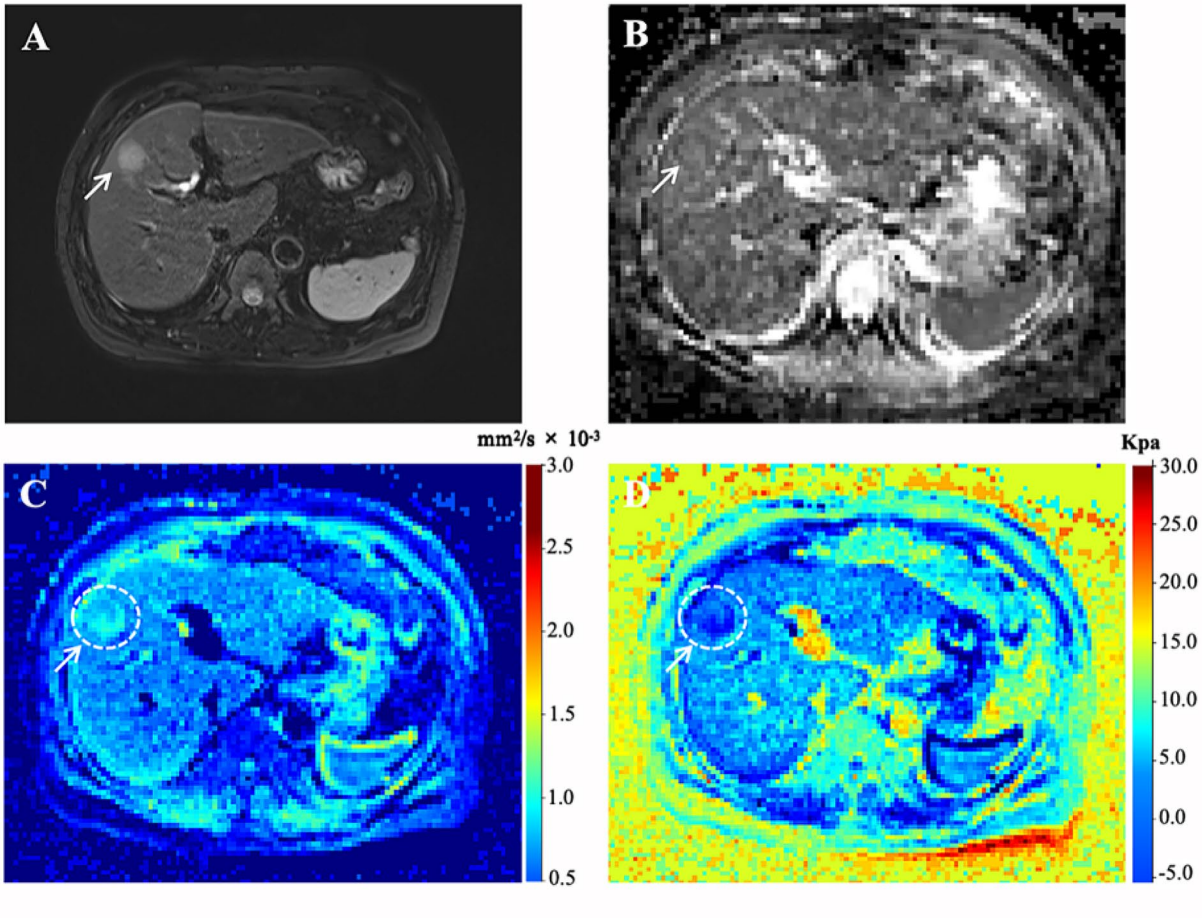

Fig. 3 Representative MR images of a 60-year-old woman with pathologically verified HCC without recurrence during a 5-year follow-up. (**A**) Axial T2-weighted image shows a hyperintensity mass (arrow) on segment VIII of liver. (**B**-**D**) ADC, sADC, and μ_{diff} maps showing that the mean ADC, sADC, and μ_{diff} values of the tumor (arrow) were 1.35×10^{-3} mm^2/s, 0.94×10^{-3} mm^2/s, and 1.99 kPa, respectively. ADC, apparent diffusion coefficient; sADC, shifted apparent diffusion coefficient; μ_{diff}, DWI-based virtual shear modulus

alone ($p=0.016$). ROC analyses showed that the performance of μ_{diff} alone in predicting recurrence in HCC was similar to that of the preoperative model ($p=0.334$) and the pre- and postoperative models showed comparable performance ($p=0.137$). More details about the diagnostic performance are summarized in Table 4.

Histopathological characteristics

The correlations between the μ_{diff} values and histopathological characteristics of HCC lesions are showed in Fig. 6. The mean values of μ_{diff} of CK19-positive HCCs were significantly higher than the CK19-negative HCCs (3.95 ± 2.37 vs. 3.15 ± 1.77, $p=0.017$). In addition, the HCC lesions with high expression of Ki-67 also showed significantly higher μ_{diff} values (4.22 ± 1.63 vs. 2.72 ± 2.12, $p=0.001$). There were no statistical differences of the μ_{diff} values in the HCC lesions classified by the remaining histopathological characteristics.

Discussion

In this study, our results demonstrated that the μ_{diff} values and corona enhancement were independent risk factors for predicting RFS of HCC patients. More pertinently, we found that the HCC patients with higher μ_{diff} values and corona enhancement tended to have a higher incidence of HCC recurrence. Furthermore, the higher μ_{diff} values were associated with expression of CK19 and high Ki-67 labeling index of HCC.

Previously published studies emphasized the value of tumor stiffness evaluated by MRE for prediction of the tumor recurrence of HCC after hepatectomy [9, 14, 15]. Wang et al. [14] reported that tumor stiffness measured by MRE was independently associated with early recurrence of HCC. In addition, Park et al. [15] also revealed that the MRE-based tumor stiffness was a significant predictive factor for RFS of HCC patients after hepatectomy. In theory, tumor invasion and metastasis in HCC are facilitated by higher tumor stiffness, which

Table 3 Univariate and multivariate Cox proportional hazards regression analyses of risk factors for recurrence of HCC

Risk Factors	Univariate Analysis		Multivariate Analysis			
			preoperative model		postoperative model	
	HR (95% CI)	*p value*	*HR (95% CI)*	*p value*	*HR (95% CI)*	*p value*
Age (years)	1.00 (0.96–1.03)	0.874				
Gender of male	0.51 (0.24–1.12)	0.095				
AFP > 20 ng/ml	0.69 (0.35–1.33)	0.266				
CEA > 5 ng/ml	0.77 (0.24–2.52)	0.667				
CA19-9 > 34 U/ml	1.54 (0.76–3.12)	0.227				
Total bilirubin > 20.4 μmol/L	1.56 (0.60–4.07)	0.359				
Alanine aminotransferase level > 50 U/L	0.87 (0.36–2.10)	0.758				
Aspartate aminotransaminase level > 40 U/L	1.17 (0.58–2.34)	0.674				
Tumor diameter	0.95 (0.85–1.07)	0.428				
Intratumoral hemorrhage	0.51 (0.15–1.66)	0.261				
Intratumoral fat	0.57 (0.17–1.85)	0.347				
Tumor margin	1.98 (0.82–4.76)	0.129				
Corona enhancement	2.61 (1.32–5.17)	**0.006**	2.25 (1.10–4.59)	**0.026**	1.36 (0.57–3.25)	0.483
Targetoid appearance	2.10 (1.06–4.15)	**0.033**	1.70 (0.82–3.53)	0.156	1.53 (0.68–3.41)	0.302
Liver fibrosis stage	1.16 (0.56–2.42)	0.70				
ADC	0.99 (0.99-1.00)	0.340				
ADC_{liver}	0.99 (0.99-1.00)	0.957				
μ_{diff}	1.39 (1.18–1.64)	**< 0.001**	1.30 (1.09–1.54)	**0.003**	1.23 (1.01–1.50)	**0.037**
$\mu_{diff-liver}$	0.98 (0.80–1.21)	0.874				
CK19	1.80 (0.92–3.51)	0.084				
KI-67	2.59 (1.31–5.13)	**0.006**	NA	NA	1.15 (0.52–2.57)	0.730
MVI	5.65 (2.71–11.78)	**< 0.001**	NA	NA	2.86 (1.10–7.46)	**0.019**
Hitological tumor grade	2.38 (1.21–4.69)	**0.012**	NA	NA	2.07 (1.01–4.23)	**0.047**

AFP: alpha-fetoprotein; ADC: apparent diffusion coefficient; μ_{diff}: DWI-based virtual shear modulus; MVI: microvascular invasion; NA: not applicable

Data in parentheses are 95% CI. Each variable with $P<0.05$ at univariate analysis was entered into the multivariate analysis

is driven by increased extracellular matrix (ECM) rigidity due to excessive collagen deposition and crosslinking of extracellular matrix proteins [16, 17]. The ECM plays an important role in promoting tumor cell proliferation, differentiation and chemotherapeutic resistance, resulting in increased tumor stiffness and poor prognosis [18]. Therefore, preoperative evaluation of tumor stiffness might have potential benefits for improving long-term prognosis of HCC patients. However, clinical application for MRE is limited due to the need for extra equipment, the dedicated MRI sequence and longer acquisition times. In recent years, studies showed the possibility of the DWI-based virtual MRE for assessment of liver fibrosis [10, 11], which was also confirmed in the present study. Ota T et al. [19] demonstrated there were strong correlations between sADC values and the MRE-based stiffness values both in the liver parenchyma and liver tumors [19], which suggests the possibility of using the vMRE-derived μ_{diff} values for preoperative evaluation of tumor characteristics of HCC. In the present study, we explored the relationship between the vMRE parameters and prognosis of HCC patients and found higher μ_{diff} values were an independent risk factor for predicting RFS of HCC patients after surgical resection. We speculate this might be attribute to the higher stiffness caused by the significant cell proliferation in more aggressive HCC [20]. The use of vMRE as a complement to MRE is intriguing and may have potential clinical value in treatment optimization for HCC patients. In contrast to MRE, the vMRE can be easily incorporated into routine MRI scan protocols with a simple workflow and short acquisition time.

Another interesting result of this study is that the higher μ_{diff} values were found to be associated with the expression of CK19 and high Ki-67 labeling index of HCC. The CK19-positive HCC shows abundant fibrous stroma which may result in increased cellularity and stiffness [21]. The Ki-67 labeling index can reflect the level of tumor proliferation. The HCC lesions with high Ki-67 labeling index showed faster cell proliferation than those with low Ki-67 labeling index during tumorigenesis, which resulted in increased nucleus/cytoplasm ratio and decreased extracellular/intracellular space. Both of these two histopathological characteristics can lead to increased μ_{diff} values, which have the potential to noninvasively reveal the cellularity and stiffness in HCC lesions. The association between μ_{diff} values and the expression CK19 and high Ki-67 labeling index of HCC lesions might explain why HCC patients with higher μ_{diff} values have a shorter RFS. The mean ADC values in our

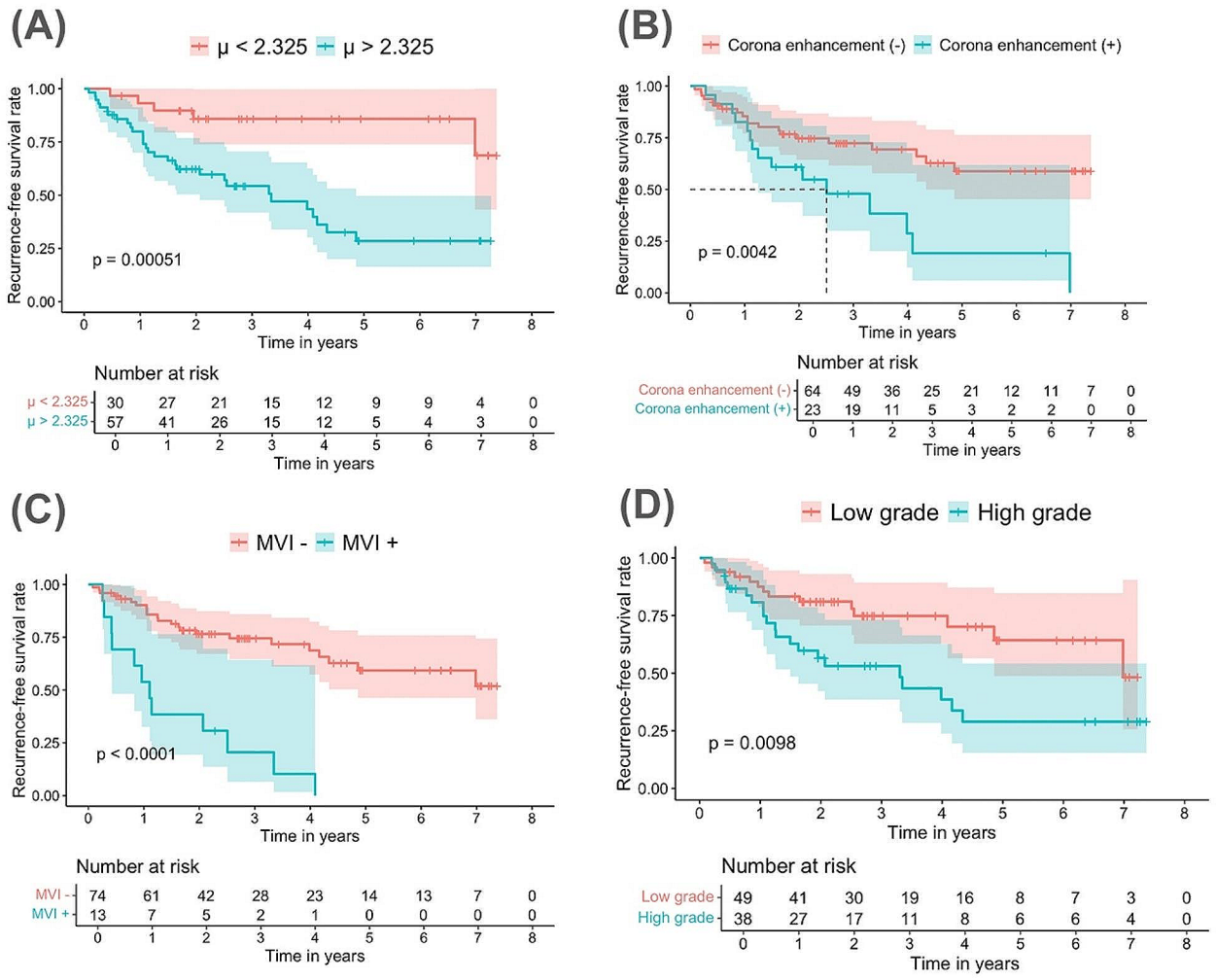

Fig. 4 Recurrence-free survival (RFS) outcome. (**a**) The Kaplan–Meier analysis shows that the patients with μ_{diff} values > 2.325 kPa have lower RFS rates than patients with μ_{diff} values ≤ 2.325 kPa; (**b**) Patients with corona enhancement HCC lesions have lower RFS rates than patients without corona enhancement HCC lesions. (**c**) Patients with MVI-positive HCC lesions have lower RFS rates than patients without MVI. (**c**) Patients with high histologic tumor grade have lower RFS rates than patients with low histologic tumor grade

RFS: recurrence-free survival; ADC: apparent diffusion coefficient; μ_{diff}: DWI-based virtual shear modulus; HCC: hepatocellular carcinoma; MVI: microvascular invasion

study had no correlation with tumor recurrence which is in accordance with studies reported by Chuang et al. [22] and Nakanishi et al. [23]. The ADC values derived from conventional monoexponential diffusion with two relatively low b-values was based on the assumption of the simple Gaussian diffusion behavior, which is inherently defective for heterogeneous tumor tissues. This might be the reason why previous research indicated controversial conclusions in the prediction of HCC recurrence [22–24]. By using higher b-values (b = 200, 1500 s/mm^2), the vMRE can reflect both Gaussian and non-Gaussian diffusion with increased sensitivity to tissue microstructure, thereby reaching better diagnostic efficiency in the prediction of prognosis of HCC.

The value of morphological features in MRI in prediction of prognosis of HCC patients have been widely reported. In our study, we found that the corona enhancement was an independent risk factor for predicting HCC recurrence in preoperative model. This finding was consistent with research reported by Wei et al. [25] and An et al. [26]. The presence of corona enhancement is caused by disordered venous drainage that develops during tumorigenesis due to obstruction of intratumoral hepatic veins, indicating a propensity to infiltrate drainage vessels of the tumor, leading to intrahepatic metastases [27–29]. The MVI and histologic grade has been widely reported and established as significant risk factors of postoperative recurrence [30, 31], which was also confirmed in the present study. By adding the pathological

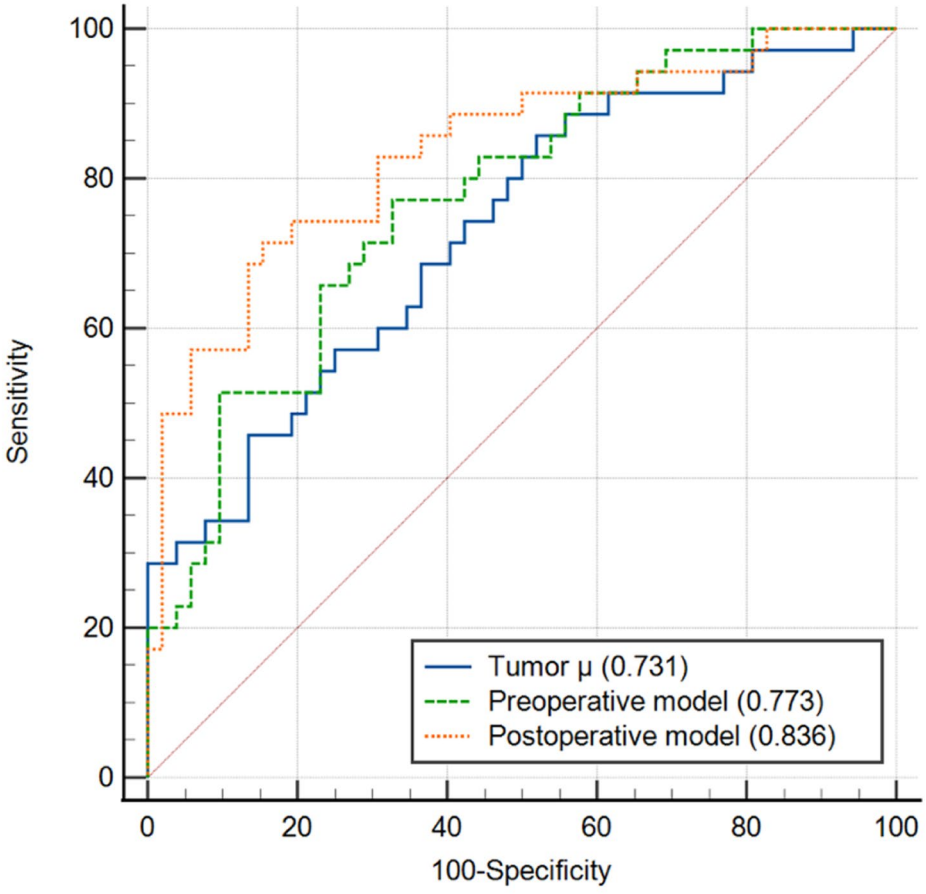

Fig. 5 Graph indicating the ROC curves for μ_{diff}, preoperative model and postoperative model for predicting HCC recurrence after hepatectomy. The AUCs for the corresponding ROC curves were 0.731 (μ_{diff}), 0.773 (preoperative model), and 0.836 (postoperative model). AUC: Area under the curve; HCC: hepatocellular carcinoma; ROC: receiver operating characteristic; μ_{diff}: DWI-based virtual shear modulus

Table 4 Diagnostic performance for predicting recurrence of HCC

Parameters	Variables	AUC (95% CI)	Sensitivity (%)	Specificity (%)	Accuracy (%)	PPV	NPV
μ_{diff}	/	0.731 (0.626–0.821)	85.71	48.08	63.22	52.63	83.33
Preoperative model	μ_{diff}, corona enhancement	0.773 (0.670–0.856)	77.01	67.31	71.27	61.36	81.40
Postoperative model	μ_{diff}, MVI and histologic tumor grade	0.836 (0.741–0.907)	71.43	84.62	79.31	75.76	81.48

Data are presented as percentages. Data in parentheses are the number of subjects used to calculate the percentage

μ_{diff}: DWI-based virtual shear modulus. AUC: areas under the ROC curve; 95% CI: 95% confidence interval; PPV: positive predictive value; NPV: negative predictive value. MVI: microvascular invasion

characteristics, the postoperative model demonstrated best diagnostic efficiency which is significantly higher compared with using μ_{diff} alone. The pre- and postoperative models showed comparable performance for predicting RFS. This may render the findings more meaningful in clinical practice. The patients in the very early stage who received radiofrequency ablation without pathological information might benefit from the preoperative model by allowing reappraisal of tumor biology. However, the value of vMRE parameter in predicting the prognosis of patients with different therapeutic tools for HCC need further study in the future.

Our study had several limitations. First, the retrospective nature of this study may have introduced a selection bias and the sample size is relatively small. Second, a previous study reported by Hanniman et al. [32] found that the fat-corrected vMRE was not associated with fibrosis stage in Non-alcoholic fatty liver disease. Since the most of the study population were infected by HBV, whether the vMRE can be used for predicting prognosis in HCC patients caused by other etiologies need further investigation. Third, the patients in this study did not take the MRE examination, and the direct correlations between the μ_{diff} values and MRE-based stiffness values of the tumors should be testified in a larger prospective cohort.

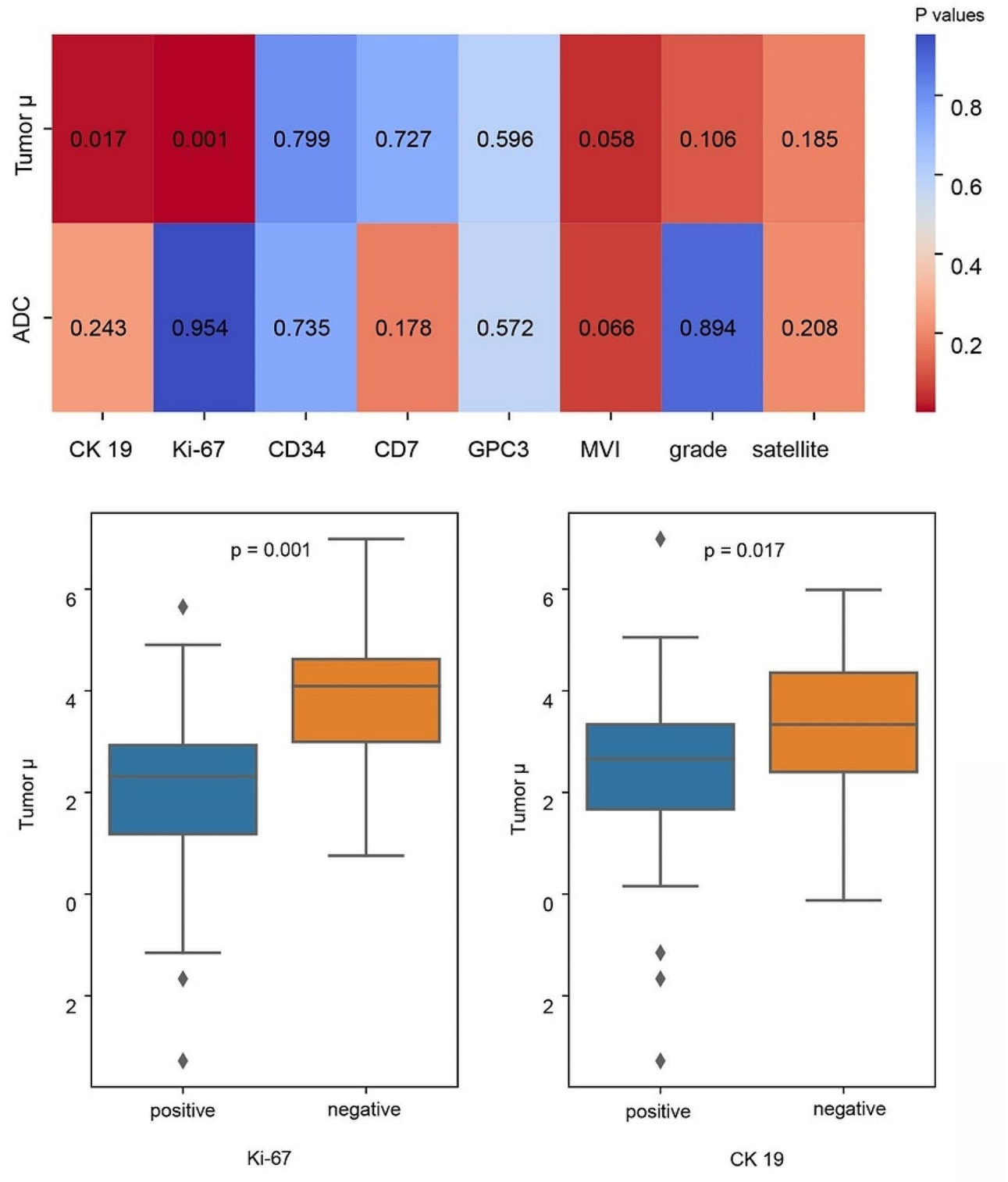

Fig. 6 The correlation between quantitative parameters and histopathological characteristics of HCC. (**a**) The heat map shows the *P* values of both ADC and μ_{diff} values in HCC lesions with or without different histopathological characteristics. (**b**) The Box-and-whisker plots show distributions of μ_{diff} values in HCC lesions with or without expression of CK19 and high Ki-67 labeling index of HCC. ADC: apparent diffusion coefficient; μ_{diff}: DWI-based virtual shear modulus; HCC: hepatocellular carcinoma

Finally, the identified optimal cut-off values of the μ_{diff} values in our study were not tested in a separate validation cohort due to relatively small sample size. Future studies with larger number of patients in a multicenter setting are warranted.

Conclusion

In conclusion, the vMRE is a promising tool for prediction of HCC recurrence after hepatectomy. Patients with higher μ_{diff} values may need more regular follow-up to detect tumor recurrence in the early stage, thus achieving a better prognosis.

Abbreviations

AUC	Area under the receiver operating characteristic curve
CK19	Cytokeratin 19
HCC	Hepatocellular carcinoma
HR	Hazard ratio
RFS	Recurrence-free survival
sADC	Shifted apparent diffusion coefficient
vMRE	Diffusion–based virtual MR elastography

Supplementary Information

The online version contains supplementary material available at https://doi.org/10.1186/s40644-024-00759-8.

Supplementary Material 1

Author contributions

All authors are aware of and agree to the submission and that they have all contributed to the work described sufficiently to be named as authors. Jiejun Chen and Sun Wei was responsible for manuscript writing and statistical analysis. Wentao Wang contributed to clinical data collection. Caixia Fu and Robert Grimm helped for image analysis technique. Mengsu Zeng helped for improvement of article structure. Sheng-xiang Rao designed the study, and revised the manuscript.

Funding

This work was supported by funds from the National Natural Science Foundation of China (82272078).

Data availability

The datasets used and/or analysed during the current study are available from the corresponding author on reasonable request.

Declarations

Ethics approval and consent to participate

This retrospective study was approved by the medical ethics committee of our institution. This work was performed in adherence to the tenets of the Declaration of Helsinki.

Consent for publication

Not applicable.

Competing interests

The authors declare no competing interests.

Received: 18 February 2024 / Accepted: 7 August 2024
Published online: 13 August 2024

References

1. Siegel RL, Miller KD, Fuchs HE, Jemal A, Cancer Statistics. 2021. CA Cancer J Clin 2021;71:7–33.
2. Vogel A, Meyer T, Sapisochin G, Salem R, Saborowski A. Hepatocellular carcinoma. Lancet. 2022;400:1345–62.
3. Cheng Z, Yang P, Qu S, Zhou J, Yang J, Yang X, Xia Y, et al. Risk factors and management for early and late intrahepatic recurrence of solitary hepatocellular carcinoma after curative resection. HPB (Oxford). 2015;17:422–7.
4. Li T, Qin LX, Gong X, Zhou J, Sun HC, Wang L, Qiu SJ, et al. Clinical characteristics, outcome, and risk factors for early and late intrahepatic recurrence of female patients after curative resection of hepatocellular carcinoma. Surgery. 2014;156:651–60.
5. Shuyao W, Mingyang B, Feifei M, Xiaoqin H. CK19 predicts recurrence and prognosis of HBV positive HCC. J Gastrointest Surg. 2022;26:341–51.
6. Lei HJ, Wang SY, Chau IY, Li AF, Chau YP, Hsia CY, Chou SC, et al. Hepatoma upregulated protein and Ki-67 expression in resectable hepatocellular carcinoma. J Chin Med Assoc. 2021;84:623–32.
7. Lee YJ, Lee JM, Lee JS, Lee HY, Park BH, Kim YH, Han JK, et al. Hepatocellular carcinoma: diagnostic performance of multidetector CT and MR imaging-a systematic review and meta-analysis. Radiology. 2015;275:97–109.
8. Hennedige TP, Hallinan JT, Leung FP, Teo LL, Iyer S, Wang G, Chang S, et al. Comparison of magnetic resonance elastography and diffusion-weighted imaging for differentiating benign and malignant liver lesions. Eur Radiol. 2016;26:398–406.
9. Zhang L, Chen J, Jiang H, Rong D, Guo N, Yang H, Zhu J, et al. MR elastography as a biomarker for prediction of early and late recurrence in HBV-related hepatocellular carcinoma patients before hepatectomy. Eur J Radiol. 2022;152:110340.
10. Le Bihan D, Ichikawa S, Motosugi U. Diffusion and intravoxel incoherent motion MR imaging-based virtual elastography: a hypothesis-generating study in the liver. Radiology. 2017;285:609–19.
11. Kromrey ML, Le Bihan D, Ichikawa S, Motosugi U. Diffusion-weighted MRI-based virtual elastography for the assessment of liver fibrosis. Radiology. 2020;295:127–35.
12. Durnez A, Verslype C, Nevens F, Fevery J, Aerts R, Pirenne J, Lesaffre E, et al. The clinicopathological and prognostic relevance of cytokeratin 7 and 19 expression in hepatocellular carcinoma. A possible progenitor cell origin. Histopathology. 2006;49:138–51.
13. Roayaie S, Blume IN, Thung SN, Guido M, Fiel MI, Hiotis S, Labow DM, et al. A system of classifying microvascular invasion to predict outcome after resection in patients with hepatocellular carcinoma. Gastroenterology. 2009;137:850–5.
14. Wang J, Shan Q, Liu Y, Yang H, Kuang S, He B, Zhang Y, et al. 3D MR elastography of hepatocellular carcinomas as a potential biomarker for predicting tumor recurrence. J Magn Reson Imaging. 2019;49:719–30.
15. Park SJ, Yoon JH, Lee DH, Lim WH, Lee JM. Tumor stiffness measurements on MR elastography for single nodular hepatocellular carcinomas can predict tumor recurrence after hepatic resection. J Magn Reson Imaging. 2021;53:587–96.
16. Dong Y, Zheng Q, Wang Z, Lin X, You Y, Wu S, Wang Y, et al. Higher matrix stiffness as an independent initiator triggers epithelial-mesenchymal transition and facilitates HCC metastasis. J Hematol Oncol. 2019;12:112.
17. Wei SC, Fattet L, Tsai JH, Guo Y, Pai VH, Majeski HE, Chen AC, et al. Matrix stiffness drives epithelial-mesenchymal transition and tumour metastasis through a TWIST1-G3BP2 mechanotransduction pathway. Nat Cell Biol. 2015;17:678–88.
18. Schrader J, Gordon-Walker TT, Aucott RL, van Deemter M, Quaas A, Walsh S, Benten D, et al. Matrix stiffness modulates proliferation, chemotherapeutic response, and dormancy in hepatocellular carcinoma cells. Hepatology. 2011;53:1192–205.
19. Ota T, Hori M, Le Bihan D, Fukui H, Onishi H, Nakamoto A, Tsuboyama T et al. Diffusion-based virtual MR elastography of the liver: can it be extended beyond liver fibrosis? J Clin Med. 2021;10.
20. Affo S, Yu LX, Schwabe RF. The role of cancer-associated fibroblasts and fibrosis in liver cancer. Annu Rev Pathol. 2017;12:153–86.
21. Kim H, Choi GH, Na DC, Ahn EY, Kim GI, Lee JE, Cho JY, et al. Human hepatocellular carcinomas with stemness-related marker expression: keratin 19 expression and a poor prognosis. Hepatology. 2011;54:1707–17.
22. Chuang YH, Ou HY, Yu CY, Chen CL, Weng CC, Tsang LL, Hsu HW, et al. Diffusion-weighted imaging for identifying patients at high risk of tumor recurrence following liver transplantation. Cancer Imaging. 2019;19:74.

23. Nakanishi M, Chuma M, Hige S, Omatsu T, Yokoo H, Nakanishi K, Kamiyama T, et al. Relationship between diffusion-weighted magnetic resonance imaging and histological tumor grading of hepatocellular carcinoma. Ann Surg Oncol. 2012;19:1302–9.
24. Lee S, Kim SH, Hwang JA, Lee JE, Ha SY. Pre-operative ADC predicts early recurrence of HCC after curative resection. Eur Radiol. 2019;29:1003–12.
25. Wei H, Jiang H, Zheng T, Zhang Z, Yang C, Ye Z, Duan T, et al. LI-RADS category 5 hepatocellular carcinoma: preoperative gadoxetic acid-enhanced MRI for early recurrence risk stratification after curative resection. Eur Radiol. 2021;31:2289–302.
26. An C, Kim DW, Park YN, Chung YE, Rhee H, Kim MJ. Single hepatocellular carcinoma: preoperative MR imaging to predict early recurrence after curative resection. Radiology. 2015;276:433–43.
27. Choi JY, Lee JM, Sirlin CB. CT and MR imaging diagnosis and staging of hepatocellular carcinoma: part I. Development, growth, and spread: key pathologic and imaging aspects. Radiology. 2014;272:635–54.
28. Choi JY, Lee JM, Sirlin CB. CT and MR imaging diagnosis and staging of hepatocellular carcinoma: part II. Extracellular agents, hepatobiliary agents, and ancillary imaging features. Radiology. 2014;273:30–50.
29. Cerny M, Chernyak V, Olivié D, Billiard JS, Murphy-Lavallée J, Kielar AZ, Elsayes KM et al. LI-RADS version 2018 ancillary features at MRI. Radiographics. 2018;38:1973–2001.
30. Lee S, Kang TW, Song KD, Lee MW, Rhim H, Lim HK, Kim SY, et al. Effect of microvascular invasion risk on early recurrence of hepatocellular carcinoma after surgery and radiofrequency ablation. Ann Surg. 2021;273:564–71.
31. Zhou L, Rui JA, Zhou WX, Wang SB, Chen SG, Qu Q. Edmondson-Steiner grade: a crucial predictor of recurrence and survival in hepatocellular carcinoma without microvascular invasio. Pathol Res Pract. 2017;213:824–30.
32. Hanniman E, Costa AF, Bowen CV, Abdolell M, Stueck A, McLeod M, Peltekian K, et al. Prospective evaluation of virtual MR elastography with diffusion-weighted imaging in subjects with nonalcoholic fatty liver disease. J Magn Reson Imaging. 2022;56:1448–56.

Publisher's Note